IJCRT.ORG ISSN : 2320-2882

INTERNATIONAL JOURNAL OF CREATIVE RESEARCH THOUGHTS (IJCRT)

An International Open Access, Peer-reviewed, Refereed Journal

Experimental Investigation Of Wear Characteristics Of Wire Arc Addictive Manufactured Inconel Alloy

[1]Mahammad Sulthan Ali ,Mr. K. Sreenivasa Reddy [*2]

[1]M.Tech Student in Mechanical Engineering, Godavari Global University, Rajamahendravaram, Andhra Pradesh, India.

[2]Assistant Professor in Mechanical Engineering, Godavari Global University, Rajamahendravaram, Andhra Pradesh, India.

ABSTRACT

Inconel 625 is widely used in aerospace, marine, and chemical industries owing to its exceptional corrosion resistance and high-temperature strength; however, its poor machinability and moderate wear resistance limit broader structural applications. Wire and arc additive manufacturing (WAAM) offer a cost-effective route for fabricating large-scale Inconel 625 components but tailoring their surface and bulk properties through in-situ reinforcement remains underexplored. This study addresses this gap by incorporating Titanium Carbide (TiC) particles (1–4 wt.%) into the melt pool using a dedicated powder feeder during vertical WAAM deposition, enabling uniform reinforcement without disrupting the process. The effect of TiC addition on hardness, tensile behavior, impact toughness, and wear resistance was systematically investigated. Hardness increased steadily with reinforcement, reaching 342.8 HV at 4 wt.% TiC (~22% higher than the base alloy), while ultimate tensile strength improved by 8–12%, with a peak value of 712.8 MPa for 3 wt.% TiC. Pin-on-disc tests under 1– 3 kg loads showed up to ~32% reduction in cumulative wear loss compared to the unreinforced alloy, confirming the role of TiC in enhancing surface durability. However, impact toughness decreased by 15–56% with increasing TiC content, indicating a trade-off between strengthening and ductility. These findings demonstrate that in-process TiC reinforcement during WAAM provides a robust pathway to simultaneously improve mechanical performance and wear resistance of Inconel 625, expanding its applicability in demanding engineering environments.

KEY WORDS: Wire Arc Additive Manufacturing, Ceramic Powder, Layer by Layer manufacturing, Inconel 625.

LITERATURE REVIEW

[1] In this work, **Rooprai et al.** developed Inconel 625 clads on EN-8 steel using a hybrid-mode WAAM-CMT process with TiC powder additions of 10, 20, and 30 wt%. The study is motivated by the severe abrasive wear experienced by agricultural tillage tools and the need for a high-performance, yet economical, surface layer. The authors systematically compare abrasive wear behaviour and coefficient of friction for different TiC contents and sample orientations. Clads with 30 wt% TiC exhibited the highest microhardness and the best abrasive wear resistance, attributed to a higher fraction of hard TiC particles and elongated dendrites in the nickel-based matrix. However, the coefficient of friction increased with TiC content, highlighting a trade-off between wear resistance and frictional losses. Obliquely oriented samples showed superior wear resistance due to irregular and stronger grain orientation relative to the wear direction. SEM and EDS analyses revealed mixed wear mechanisms: plastic deformation and furrowing in Inconel-rich regions, and minimal penetration in high-TiC zones. Overall, this paper demonstrates that blending ceramic reinforcements into WAAM Inconel 625 is an effective strategy to extend the service life of EN-8 based tillage tools while emphasizing the need to optimize TiC level and loading direction.

[2] **Rodrigues et al**. proposed a novel grain-refinement strategy for Inconel 625 parts produced by WAAM using in-situ addition of TiB_2 particles. The key innovation is an actuator system that injects a TiB_2-containing solution with a volatile flux; the flux evaporates before reaching the arc, leaving TiB_2 particles to adhere to the wire or be transported by the shielding gas into the molten pool. TiB_2 was added at 0.31 and 0.56 wt%, and the resulting microstructure and mechanical properties were compared with a reference as-built WAAM Inconel 625. EBSD analysis showed a strong columnar-to- equiaxed grain transformation upon TiB_2 addition, with the average grain area decreasing from 1823 μm^2 in the reference sample to 583 μm^2 at 0.56 wt% TiB_2. The size of interdendritic segregation regions was also significantly reduced, indicating more homogeneous solidification. Synchrotron X-ray diffraction was used to assess residual stresses and phase content, confirming that the refinement did not introduce deleterious phases. Mechanical testing revealed an increase in strength primarily attributed to Hall–Petch strengthening from grain refinement, without a significant loss of ductility. This paper highlights inoculant-based grain refinement as a process-independent, geometry-independent route to overcome the typical coarse, textured microstructure of WAAM Inconel 625.

[3] **Bölükbaşı et al**. investigated the use of pack aluminizing to enhance high- temperature oxidation resistance of WAAM-fabricated Inconel 625. WAAM IN625 samples were aluminized at 700 °C for 3 h, producing a continuous ~35 μm thick aluminide coating. XRD and SEM/EDS characterisation showed that the coating is primarily composed of NiAl, Ni_2Al_3, Cr_2Al, and $MoAl_5$ phases, with a significantly increased nano-hardness (≈12.85 GPa). The authors conducted isothermal oxidation tests in air at 1000 °C for 5, 25, and 50 h, comparing aluminized and as-built conditions. Aluminized specimens exhibited substantially lower mass gain and oxide scale growth, with oxidation resistance 6.63 times, 2.70

times, and 2.65 times higher than as-built WAAM IN625 at 5, 25, and 50 h, respectively. The improved behaviour is linked to the stability of aluminide phases and the formation of a protective Al_2O_3-rich scale, whereas as-built samples transitioned from a Cr_2O_3-dominated scale to mixed spinel oxides such as $NiCr_2O_4$, $NiMoO_4$ and NiO at longer times. The study also notes that prolonged exposure leads to Kirkendall void formation and degradation within the aluminized layer, indicating an upper limit to long-term exposure.

[4] **Sharma et al.** examined how different post-heat treatments influence the metallurgical, mechanical, and corrosion behaviour of WAAM-CMT Inconel 625 builds. As-deposited walls were subjected to multiple heat-treatment schedules, including solutionising up to 1100 °C followed by different cooling routes, and compared with the as-built condition. Metallurgical characterisation using EBSD, SEM-EDS, and XRD highlighted changes in grain morphology, texture, and secondary phase distribution after heat treatment. Mechanical testing (tensile and impact) showed that an appropriate high-temperature treatment (1100 °C for 2 h followed by water quenching) significantly improved yield and tensile strength while maintaining or enhancing impact toughness. Cyclic polarization tests in a corrosive medium revealed variations in pitting potential and repassivation behaviour; samples treated at 1100 °C with water quenching exhibited the best corrosion resistance, attributed to homogenisation of the microstructure and reduction of deleterious segregated phases. Fractography of failed tensile and impact specimens confirmed predominantly ductile fracture with refined dimples in optimally heat-treated samples, in contrast to more heterogeneous fracture features in the as-built alloy. This paper shows that careful selection of post-heat treatment can simultaneously optimise mechanical and corrosion performance of WAAM-CMT Inconel 625, which is crucial for service in aggressive environments.

[5] **Rodrigues et al**. produced a 316L stainless steel–Inconel 625 functionally graded material (FGM) using Twin-Wire and Arc Additive Manufacturing (T-WAAM). Two interface strategies were studied: a direct, abrupt transition and a smooth, compositionally graded transition between 316L and Inconel 625. Microstructural analysis revealed that both approaches yielded defect-free, fully bonded interfaces with an austenitic matrix across the FGM. However, the smooth gradient produced additional secondary phases such as δ-phase (Ni_3Nb) and carbides, as identified by synchrotron X-ray diffraction, which were not present in the direct interface strategy. Mechanical testing showed that the FGM with a direct interface exhibited higher tensile strength and elongation, indicating a more favourable combination of strength and ductility. Neutron diffraction measurements further indicated that lower residual stresses were present in the direct-interface FGM compared to the smooth gradient. The authors emphasised that while compositional grading can theoretically mitigate abrupt changes in properties, it may also promote undesirable phase formation in Ni-rich regions.

[6] **Amiri and Naffakh-Moosavy** fabricated a three-step functionally graded structure transitioning from plain carbon steel to 316L stainless steel and finally to Inconel 625 using WAAM. The work focuses on microstructural continuity across the gradient, defect formation, and mechanical properties of each

transition region. Microstructural observations showed a sound, defect-free metallurgical bond across both carbon- steel/316L and 316L/Inconel 625 interfaces. The 316L region exhibited a ferrite– austenite (FA) solid-state transformation with a noticeable fraction of δ-ferrite within an austenitic matrix, whereas the Inconel 625 region solidified into a dendritic γ-Ni matrix with discontinuous Laves intermetallic phases in interdendritic regions due to Nb and Mo segregation. Hardness measurements reflected the compositional gradient:

~159–170 HV in carbon steel, 171–178 HV in 316L, and 194–257 HV in Inconel 625, producing a smooth overall hardness profile. Tensile specimens failed in the carbon-steel region, indicating that both interfaces possess higher strength than the plain carbon steel substrate. Fractography revealed uniformly distributed dimples, confirming ductile failure. The study demonstrates that WAAM can produce robust multi-material FGMs that overcome many limitations of conventional fusion welding, such as brittle intermetallics and liquation cracking, in iron–nickel based multi-alloy systems.

[7] **Kishor et al**. carried out a detailed study of microstructural evolution, crystallographic texture, grain morphology, and mechanical integrity in a 60-layer Inconel 625 wall produced by CMT-based WAAM. The authors investigated through- thickness variations using optical microscopy, EBSD, and XRD, capturing the combined effects of repeated thermal cycling and solidification conditions. The build exhibited a mixture of dendritic, cellular, columnar, and equiaxed microstructures; average grain size varied markedly with height, from ~13 μm near the substrate to ~45 μm in the mid-height region, decreasing again to ~18 μm near the top. Texture analysis showed strong Cube, Cube-ND, and Cube-RD recrystallization textures at the top, with Goss, copper, F, S, and E textures dominating middle and bottom regions. XRD-based dislocation density measurements indicated the highest dislocation density in the top region and the lowest near the substrate. Mechanical testing in different orientations revealed anisotropic behaviour: ultimate tensile strength varied between ~603 and 699 MPa and yield strength between ~313 and 365 MPa, while Vickers hardness ranged from ~240 to 260 HV along the build height.

[8] **Gurmesa et al.** investigated how wire diameter influences the mechanical and microstructural properties of Inconel 625 fabricated by WAAM. WAAM builds were produced using different wire diameters, and tensile, impact toughness, and hardness responses were systematically compared. The study found a clear trend: decreasing wire diameter led to higher tensile strength and hardness but slightly reduced ductility. These changes were linked to grain refinement, as smaller wire diameters tended to produce finer grains due to modified heat input and solidification conditions. Microhardness results also reflected anisotropy, with property variations depending on build orientation and wire size. In contrast to strength and hardness, impact toughness generally increased with larger wire diameters, indicating a trade-off between static strength and dynamic toughness. Fracture surface analyses from tensile and Charpy tests revealed predominantly ductile failure, with micro-void nucleation and coalescence forming dimpled fracture surfaces. The results provide practical guidance for selecting wire diameter in WAAM Inconel 625 components to balance strength, ductility, and impact resistance for specific applications

[9] **Chen et al.** developed a TC4–316L stainless-steel functionally graded material using a double-wire WAAM system, achieving a controlled Fe increment through wire- feed modulation. The microstructure transformed from α-Ti + FeTi to Fe_2Ti + Cr_2Ti as Fe content increased, indicating strong compositional influence on phase evolution. A critical brittle zone appeared at 50 at % Fe, where cracks initiated due to Fe_2Ti enrichment. Microhardness peaked at ~945 HV at 60 at % Fe because of hard intermetallic formation. The study confirms the feasibility of Ti–steel FGMs while highlighting compositional limits that govern cracking.

[10] **Zhang et al**. fabricated an SS304–Fe40Al graded structure using dual-wire WAAM by varying Al/Fe ratios to achieve smooth compositional transitions. The microstructure evolved from γ-Fe to α-Fe and eventually to Fe_3Al and FeAl intermetallics with rising Al content. Brittle FeAl regions exhibited cracking due to low ductility and high thermal stresses. Microhardness increased from 188 HV to 558 HV along the gradient, while compressive strength decreased as aluminides dominated. Their results provide guidance for designing Fe–Al FGMs for high-temperature and oxidation-resistant applications.

[11] **Günen et al.** introduced a simultaneous homogenization–boriding treatment for WAAM-fabricated 307 stainless steel, performed at 1000 °C for 1 h. The process produced a 30 µm boride layer (FeB, Fe_2B, Cr_5B_3, MnB) while eliminating interdendritic segregation in the as-built condition. Hardness increased sharply to 21.5 GPa within the boride layer, significantly enhancing surface integrity. Wear resistance improved by 31× at room temperature and 8× at high temperature due to the hard, lubricating boride phases. This approach shows strong potential for improving WAAM stainless steel components used in abrasive environments.

[12] **Shah et al.** provided a comprehensive review of WAAM technology, discussing heat sources, process control, deposition strategies, in-process monitoring, and materials. The review highlighted key challenges such as porosity, residual stresses, geometric inaccuracy, and arc instability. WAAM's advantages—high deposition rate, low cost, and suitability for large components—were compared with PBF and other AM processes. The authors emphasized recent advancements in sensing, path optimization, defect reduction, and hybrid processes. Their review outlines the gaps and opportunities needed for industrial-scale WAAM adoption.

[13] **Kong et al**. strengthened Inconel 718 by incorporating Ti_2AlC MAX particles (5– 10 vol%) using the DED process to suppress detrimental Laves phase formation. The 10% Ti_2AlC composite displayed 70% higher yield strength and 39% higher UTS than conventional AM-In718. Microstructure analysis showed that Laves phase was replaced by beneficial (Nb,Ti)(C,N) and γ′ precipitates. Solidification modeling explained reduced Nb segregation and improved phase distribution. Their work demonstrates an effective feedstock-modification strategy for producing high- performance AM superalloys

[14] **Cai et al**. – Nickel–Aluminum Bronze/Steel Composite via WAAM (Elongated Version) Cai et al. successfully fabricated a nickel–aluminum bronze (NAB)/steel bimetallic composite using the Wire Arc Additive Manufacturing (WAAM) process, demonstrating the capability of WAAM to join dissimilar

metals with strong metallurgical integrity. Compared to conventional cast NAB, the WAAM-processed material exhibited a significantly refined microstructure, particularly in the α-Cu and β phases. This refinement is attributed to the rapid solidification and repeated thermal cycling inherent to the WAAM process, which reduce grain coarsening and promote improved phase distribution. One of the most noteworthy observations in their study was the formation of a Fe_3Al-rich interfacial metallurgical layer between the NAB and the steel substrate. This intermetallic layer acted as a strengthening zone rather than a brittle interface, enhancing structural coherence and resisting premature debonding. The presence of Fe_3Al contributed to improved load transfer across the interface and delayed structural failure during mechanical testing.Mechanically, the WAAM- fabricated composite showed substantial enhancement over conventional NAB, achieving a 51% increase in yield strength and a 30% increase in hardness.

[15] Rashid et al. reviewed WAAM processing of nickel-based superalloys such as In718, In625, Hastelloy X, C276, and Haynes 282. The paper covers heat-source selection, microstructural evolution, defect formation, and process-parameter influence. It discusses common defects—porosity, cracking, laves formation, residual stress—and evaluates mitigation methods including heat treatment, HIP, and rolling.

The review emphasizes the importance of thermal management for stable microstructure and mechanical properties. It concludes that WAAM is highly suitable for high-temperature Ni-superalloys but requires refined process control

METHODOLOGY

MATERIAL SELECTION:

Base Material:

Inconel 625 is a high-performance nickel-based superalloy widely recognized for its outstanding mechanical strength, corrosion resistance, and superior weldability, making it an ideal material for advanced manufacturing processes such as Wire Arc Additive Manufacturing (WAAM). In this study, Inconel 625 is selected as the base material due to its unique combination of solid-solution strengthening, thermal stability, and metallurgical reliability under complex loading and environmental conditions.

The alloy's exceptional strength is primarily attributed to solid-solution strengthening from its major alloying elements, molybdenum (Mo) and niobium (Nb). Unlike precipitation-hardened superalloys, Inconel 625 does not rely on age-hardening mechanisms; instead, Mo and Nb atoms distort the nickel matrix, creating a strong resistance to dislocation movement. This mechanism allows the alloy to retain high mechanical strength across a broad temperature range, particularly at elevated temperatures approaching 980 °C, where many conventional alloys experience thermal degradation. This stability is especially beneficial in components exposed to fluctuating thermal cycles, such as in WAAM, where each deposited layer experiences reheating from subsequent layers. Another critical advantage of Inconel 625 is its exceptional resistance to environmental degradation. The high chromium content promotes the formation of a protective chromium oxide layer, providing remarkable oxidation resistance during high-temperature

exposure. Simultaneously, the synergistic effects of chromium, molybdenum, and nickel impart superior resistance to pitting, crevice corrosion, stress-corrosion cracking, and general corrosion. These properties make Inconel 625 highly suitable for harsh operational environments such as marine applications, chemical processing plants, and offshore oil and gas platforms, where aggressive media such as chlorides and acidic solutions are commonly encountered.

In addition to its corrosion resistance, Inconel 625 exhibits excellent fatigue and creep resistance, enabling it to endure long-term mechanical loading, thermal cycling, and high-temperature stress without significant deformation or microstructural deterioration. This makes the alloy ideal for structural components subjected to sustained stresses over extended periods, such as heat exchanger tubes, gas turbine hardware, nuclear reactor components, and aerospace engine parts. One of the most distinctive advantages of Inconel 625, particularly relevant to this investigation, is its superior weldability. Unlike many precipitation-hardened alloys that require careful heat treatment to avoid cracking, Inconel 625 can be welded with minimal risk of solidification cracking, segregation, or heat-affected zone (HAZ) embrittlement. Its ability to maintain structural uniformity without post-weld heat treatment (PWHT) is especially advantageous for WAAM, where repeated thermal cycles during multi-layer deposition can severely affect microstructural stability in less tolerant materials. The alloy's inherent resistance to weld-induced defects makes it a reliable base material for incorporating ceramic reinforcements such as Titanium Carbide (TiC) particles.

Table : Base Material Composition

Material	Ni	Cr	Mo	Nb + Ta	Fe	Co	Mn	Si	Ti	Al	C	P	S
Wt%	58 min	20 – 23	8–10	3.15 – 4.15	≤ 5.0	≤ 1.0	≤ 0.5	≤ 0.5	≤ 0.4	≤ 0.4	≤ 0.10	≤ 0.015	≤ 0.015

Table : Mechanical Properties of Inconel 625

Property	Value
Density	**8.44 g/cm³**
Ultimate Tensile Strength (UTS)	**760–930 MPa**
Yield Strength (0.2% Proof)	**414–517 MPa**
Elongation	**30–55%**
Hardness	**220–270 HV**
Melting Range	**1290–1350 °C**
Modulus of Elasticity	**207 GPa**
Poisson's Ratio	**0.27–0.30**
Thermal Conductivity	**9.8 W/m·K**
Specific Heat	**410 J/kg·K**

Reinforcement Material:

Titanium Carbide (TiC) is an ultra-hard ceramic compound known for its high melting point (~3160 °C), excellent wear resistance, and strong chemical stability. With a cubic crystal structure and hardness

comparable to tungsten carbide, TiC performs well under extreme temperatures and abrasive conditions. When added to metal matrices like Inconel 625, it enhances hardness, strength, and wear resistance through dispersion strengthening and grain refinement. Due to these advantages, TiC is widely used in cutting tools, protective coatings, and high-performance composite materials, making it an effective reinforcement for WAAM-based components.

Table : Composition and Properties of TiC

Ti (Titanium)	C (Carbon)	Purity	Density	Melting Point
≈ 80 wt.%	≈ 20 wt.%	≥ 99% (industrial grade)	4.9 g/cm³	~3160°C

EXPERIMENTAL PROCEDURE:

The fabrication of the Inconel 625–TiC composite walls was carried out using a Wire Arc Additive Manufacturing (WAAM) system integrated with robotic motion control. The following procedure was adopted to ensure consistent deposition quality, uniform TiC incorporation, and reliable specimen generation for mechanical and microstructural evaluation. To begin with, a mild steel substrate plate was thoroughly prepared to provide a stable base for the deposition process. The surface was cleaned using a wire brush and emery paper to remove oxides, contaminants, and loose particles, followed by polishing to ensure good adhesion of the first deposited bead. The substrate was then firmly clamped on the WAAM setup to eliminate any unwanted movement during the multi-layer deposition.

Before deposition, all welding parameters—including current, voltage, wire feed rate, travel speed, and shielding gas flow rate—were carefully set based on the optimized conditions for Inconel 625. These parameters were selected to promote stable arc formation, uniform melt pool behavior, and consistent bead geometry throughout the build. A single layer of Inconel 625 was deposited across the substrate with a typical height of approximately 2.5 mm and a length of 90 mm, forming the base for subsequent layers. After the deposition of each layer, an inter-layer cooling period of about 3–5 minutes was maintained to control thermal accumulation and reduce distortion. This cooling interval helped in achieving better dimensional stability and minimized residual stresses within the wall structure.

For walls reinforced with ceramic particles, a titanium carbide (TiC) paste was prepared separately by uniformly mixing TiC powder with ethyl alcohol to form a smooth, spreadable coating. Once each deposited Inconel layer had cooled sufficiently, the TiC paste was applied evenly over the entire surface to ensure homogeneous particle

POWDER CONTENT CALCULATION:

To obtain the required TiC reinforcement levels in the WAAM-deposited Inconel 625 walls, the amount of TiC powder to be applied on each layer was calculated based on the total mass of the weld bead. The powder content was determined using the formula:

Mass of the powder (m) = Mx / 1- x

where:

- **M** = mass of the weld bead,
- **x** = desired TiC percentage (expressed as a decimal fraction).

This calculation ensures accurate addition of TiC for each reinforcement level. Based on the required compositions, the following powder quantities were determined:

- **0% TiC → 0 g**
- **1% TiC → 0.10 g**
- **2% TiC → 0.21 g**
- **3% TiC → 0.31 g**
- **4% TiC → 0.42 g**

1.1 SAMPLE PREPERATION:

After completing the WAAM deposition process, the fabricated Inconel 625– TiC walls were subjected to a series of post-processing and machining steps to achieve the required dimensional accuracy and prepare standardized specimens for mechanical and microstructural testing. These steps were carefully planned to ensure that no additional defects, residual stresses, or microstructural alterations were introduced during handling and machining.

Once the walls had cooled to room temperature, they were carefully separated from the steel substrate plate using controlled mechanical and machining techniques to avoid damage to the deposited material. The detached walls were then transferred to a CNC milling machine for surface finishing. CNC milling was employed to remove surface irregularities, weld bead undulations, and excess buildup resulting from the layer-by-layer deposition. This operation ensured that each wall attained a uniform thickness, improved flatness, and a smooth surface finish, which are essential for accurate and consistent specimen extraction. The high precision of CNC machining also contributed to achieving tight dimensional tolerances required for ASTM-standard test specimens.

Following milling, each wall was visually inspected and clearly marked according to the layout required for tensile, impact, hardness, wear, and microstructural specimens. The marking process followed relevant ASTM guidelines to ensure proper specimen dimensions and orientations. Once the marking was completed,

the individual samples were extracted using a Wire-Cut Electrical Discharge Machining (EDM) process. Wire-Cut EDM was specifically chosen because it does not rely on mechanical cutting forces or high temperatures, thereby eliminating the risk of thermal distortion, mechanical stressing, or microstructural changes that could affect test results. This method produced specimens with clean edges, minimal burr formation, and superior dimensional accuracy.

After cutting, all specimens were washed thoroughly with acetone to remove any machining residues, EDM dielectric fluids, oils, and fine metallic debris. The cleaned samples were then air-dried, carefully labelled according to their respective TiC reinforcement percentages (0%, 1%, 2%, 3%, and 4%), and stored securely to prevent contamination prior to testing. A final visual inspection was conducted to check for surface defects, dimensional deviations, or edge damage, ensuring that only high- quality specimens proceeded to testing.

This systematic post-processing and specimen preparation procedure ensured that all samples met the required standards for mechanical and microstructural evaluation, thereby maintaining consistency and reliability across the experimental analysis.

Fig : Wire Cut EDM

Fig : Samples

TESTING:

Microstructural Analysis:

Optical Microscopy (OM):

Optical microscopy was carried out on polished and etched specimens to analyze the microstructural characteristics of the WAAM-fabricated Inconel 625–TiC composites. The samples were first subjected to standard metallographic preparation and etched to reveal the underlying grain boundaries and solidification features. Under the optical microscope, the grain size, bead morphology, and inter-layer build structure were clearly observed. The etching process highlighted the dendritic growth patterns characteristic of WAAM deposition, along with any refinement introduced by the presence of TiC particles. The distribution, dispersion uniformity, and interfacial bonding of TiC within the Inconel matrix were also evaluated. Differences in microstructure among samples with varying TiC content provided insights into particle-induced grain refinement, layer bonding quality, and solidification behaviour across the fabricated walls.

Fig 3.5: Optical Microscopy

Scanning Electron Microscopy (SEM):

Scanning Electron Microscopy (SEM) was employed to examine the detailed surface morphology and microstructural characteristics of the WAAM-fabricated Inconel 625–TiC composite samples. High-resolution SEM imaging enabled precise observation of particle dispersion within the matrix, allowing the identification of uniformly distributed TiC particles as well as regions of possible agglomeration. The technique also provided clear insights into the interfacial bonding between TiC particles and the surrounding Inconel matrix, which is critical for assessing load-transfer efficiency. Additionally, SEM facilitated the detection of micro voids, pores, cracks, and other defects that may have formed during the layer-by-layer deposition process. Solidification features such as dendritic structures, melt pool boundaries, and cellular growth patterns were also visible at higher magnifications, offering a deeper understanding of the thermal behaviour and microstructural evolution in the deposited walls.

Fig : Scanning Electron Microscopy

Energy Dispersive X-ray Spectroscopy (EDS):

Energy Dispersive X-ray Spectroscopy (EDS) was carried out alongside SEM imaging to determine the elemental composition and distribution within the WAAM- fabricated Inconel 625–TiC composites. Both spot analysis and elemental mapping were performed across reinforced and unreinforced regions to identify variations in chemical composition. The mapping results confirmed the presence and spatial distribution of TiC particles, highlighting areas of uniform dispersion as well as potential clustering. EDS also enabled the verification of key alloying elements in Inconel 625, such as Ni, Cr, Mo, and Nb, ensuring that no elemental depletion or segregation occurred during deposition. The interaction between TiC particles and the surrounding nickel matrix was clearly observed through localized enrichment of titanium and carbon, indicating successful embedding and interfacial bonding. This analysis provided critical insights into the chemical homogeneity and reinforcement effectiveness within the composite structure.

Fig : Energy Dispersive X-ray Spectroscopy

MECHANICAL TESTING:

Uniaxial Tensile Test (ASTM E8/E8M):

Sub-sized tensile specimens were prepared in accordance with ASTM E8/E8M standards to ensure consistency and reliability in mechanical evaluation. All tests were carried out at room temperature using a calibrated universal testing machine (UTM). A constant crosshead speed of 2.5 mm/min was maintained throughout the test to provide uniform loading conditions. During the experiment, the tensile load and corresponding elongation were continuously recorded until fracture. Key mechanical properties namely ultimate tensile strength (UTS)**,** yield strength (0.2% proof stress)**,** and percentage elongation were extracted from the stress–strain curves.

.

Fig : Tensile Setup

Microhardness Test (ASTM E92):

Vickers microhardness testing was conducted in accordance with ASTM E92 to evaluate the hardness distribution across the WAAM-fabricated Inconel 625–TiC composite walls. A load of 300 gf with a dwell time of 15 seconds was applied to ensure precise and consistent indentation formation. Indentations were systematically placed along the cross-section of each wall, covering both the top and bottom deposition regions to capture any variations arising from thermal cycling or microstructural differences. The measured hardness values were used to assess the influence of increasing TiC content on material performance. Enhanced hardness in reinforced samples indicated contributions from dispersion hardening, grain refinement, and the presence of hard ceramic particles embedded within the nickel matrix. This analysis provided clear evidence of the strengthening mechanisms activated by TiC addition in the WAAM process.

Fig: Vickers Hardness Setup

Impact Test (ASTM A370):

Impact toughness was assessed using sub-sized Charpy V-notch specimens prepared according to the guidelines of ASTM A370. Each specimen measured 55 mm

× 10 mm × 10 mm and contained a precisely machined 45° V-notch with a depth of 2 mm, ensuring consistent stress concentration during testing. The specimens were subjected to impact loading using a

calibrated pendulum-type impact testing machine, and the absorbed impact energy was recorded directly from the machine's dial or digital output. This energy value reflects the material's ability to resist sudden fracture under high-strain-rate conditions. By comparing the results across samples with varying TiC reinforcement levels, the study evaluated the influence of ceramic particle addition on ductility, toughness, and overall fracture resistance. The reduction or enhancement in absorbed energy helped in understanding the embrittlement or strengthening mechanisms introduced by TiC within the WAAM-processed Inconel 625 matrix.

Fig : Impact Testing

Wear Test:

Fig 3.11: Wear Test

The wear behaviour of the WAAM-fabricated Inconel 625–TiC composite samples was examined using a standard pin-on-disc tribometer. Polished cylindrical pin specimens were brought into sliding contact with a hardened steel disc to simulate abrasive and adhesive wear conditions. Tests were conducted under applied normal loads of 1 kg, 2 kg, and 3 kg, while maintaining a constant sliding speed and a fixed sliding distance to ensure uniform and reproducible wear conditions. Prior to testing, each specimen was thoroughly cleaned and accurately weighed using a precision balance. After the wear run, the samples were cleaned again to remove loose debris and re-weighed to determine the weight loss, which served as the primary indicator of

wear rate. The influence of TiC reinforcement on wear resistance was assessed by comparing weight-loss values across different compositions, providing insights into the role of hard ceramic particles in improving surface durability and reducing material removal during sliding.

RESULTS & DISCUSSION

MICROSTRUCTURAL ANALYSIS:

Selective Electron Microscopy:

1. 1% TiC

The SEM analysis of the WAAM-fabricated Inconel 625–TiC composite shows a dense, well-solidified microstructure with very low porosity and smooth layer deposition. TiC particles appear as dark, angular reinforcements dispersed throughout the matrix, with some clustering due to their high melting point and limited melt stirring. Particle sizes range from about 5 to 50 µm, and several exhibit bright interfacial rims, indicating partial dissolution and carbide formation that improves metallurgical bonding. The Inconel matrix displays fine cellular-dendritic features typical of rapid WAAM cooling, with no major defects such as cracks or lack-of-fusion. Minor pores and particle pull-out pits are present but negligible.

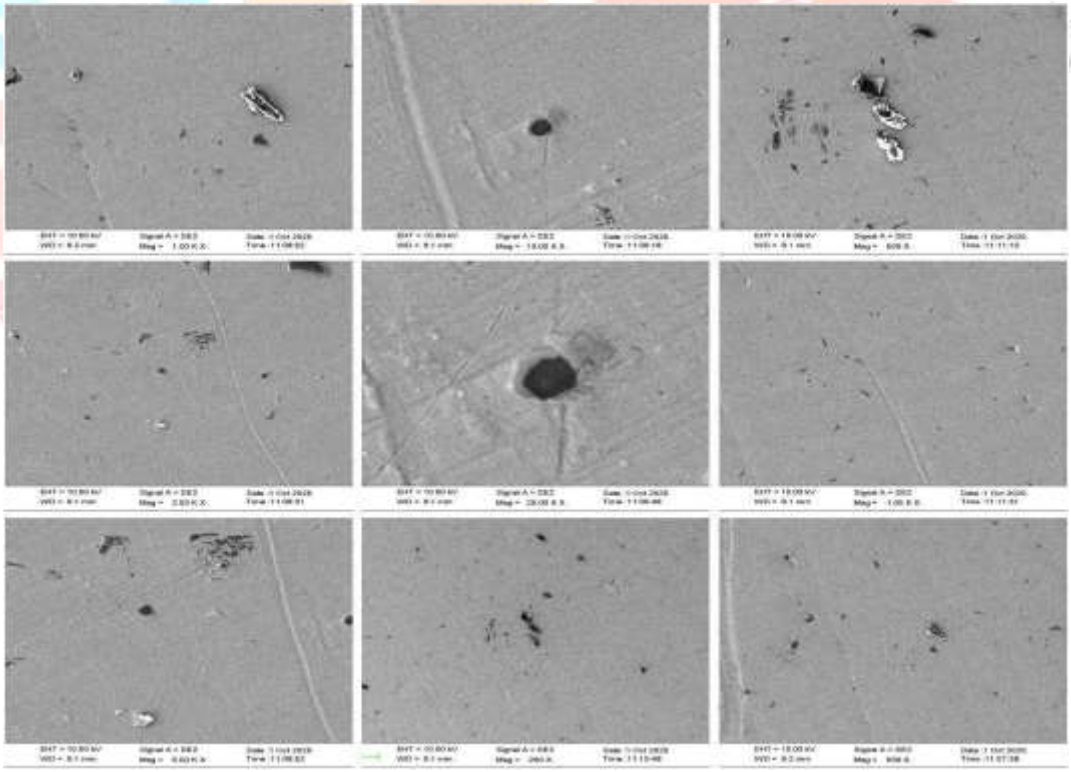

Fig : The images show uniformly solidified layers with dispersed TiC particles, minimal porosity, and stable WAAM deposition features.

2.4% TiC:

The SEM images of the WAAM-deposited Inconel 625 with 4% TiC show a dense and uniform microstructure with very minimal porosity, indicating stable deposition. TiC particles are clearly visible as dark, angular reinforcements, with higher particle concentration than lower-TiC samples. Some clustering occurs, but overall distribution remains effective. Several particles exhibit bright interfacial rims, suggesting partial dissolution and good metallurgical bonding with the Inconel matrix. The matrix appears fine and homogeneous with slight dendritic traces from rapid cooling, and no major defects such as cracks or lack-of-fusion regions are observed. Overall, the 4% TiC composite shows successful reinforcement incorporation, strong particle–matrix bonding, and a well-consolidated WAAM microstructure.

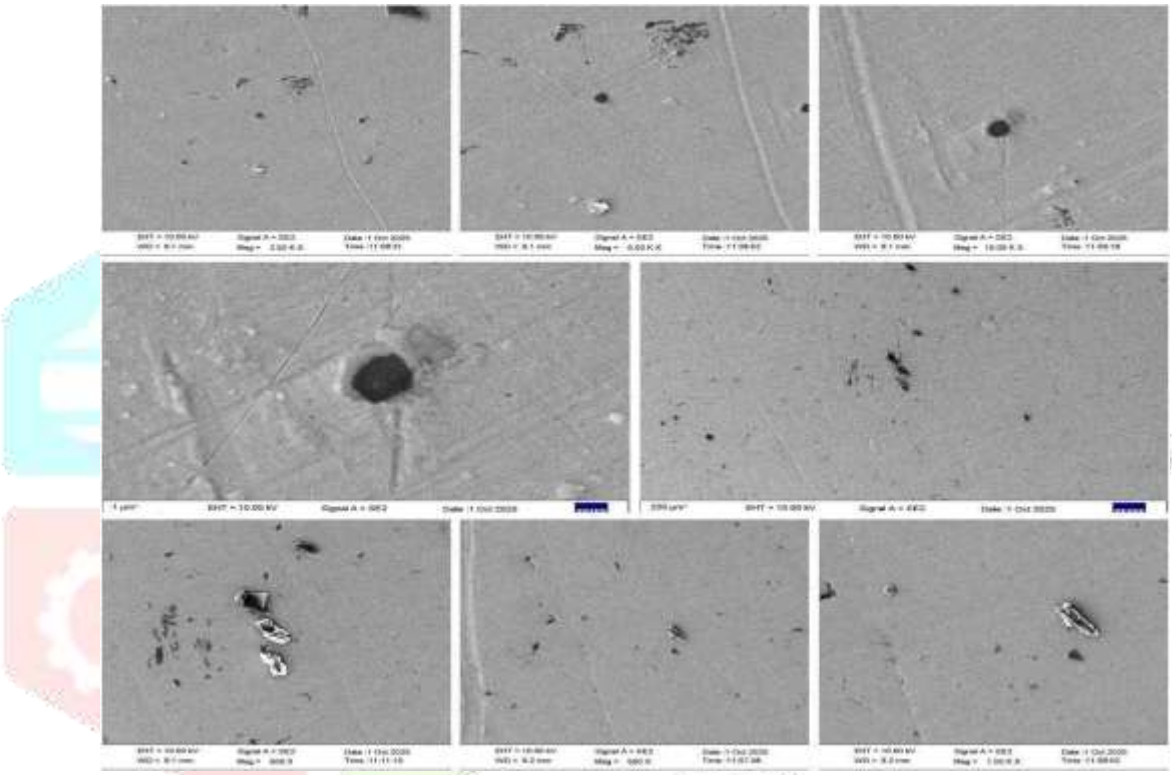

Fig: The images reveal higher TiC particle concentration, good metallurgical bonding, and a dense microstructure with negligible defects.

Energy Dispersive X-ray Spectroscopy (EDS):

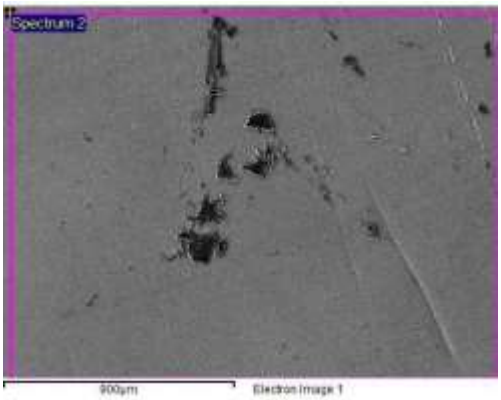

Fig: Electron Image of 1% Tic

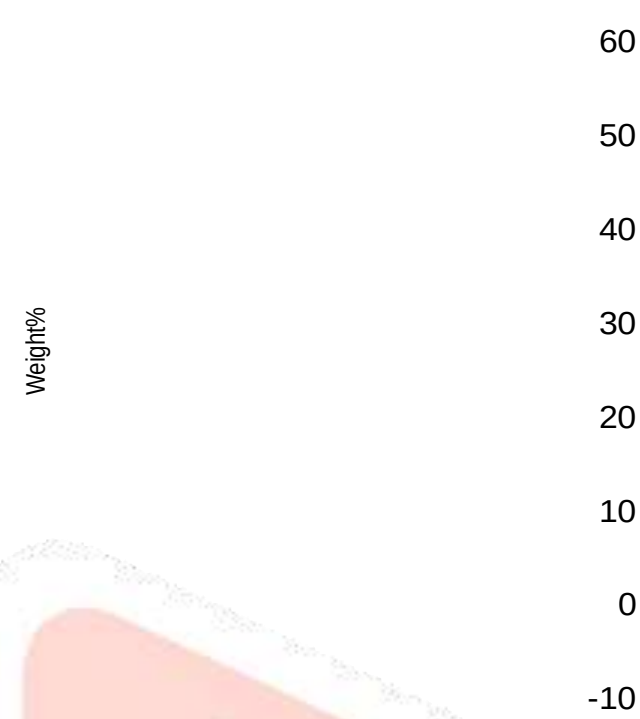

Fig: Graph of Element wt %

Quantitative results

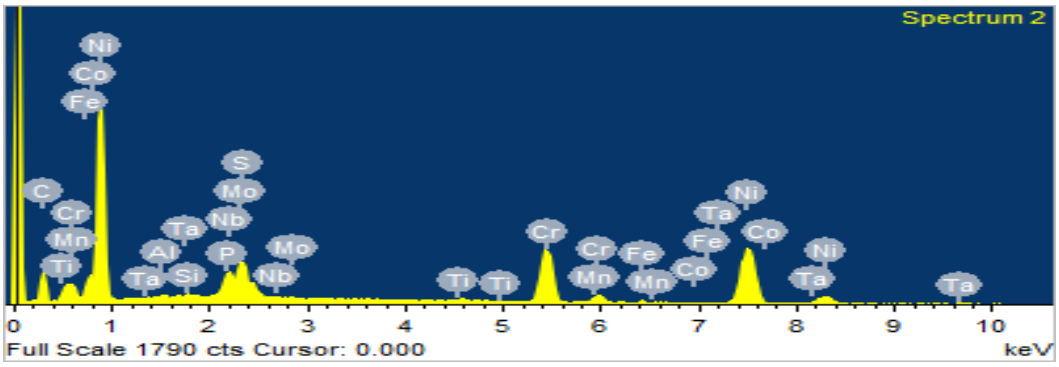

Fig : graph of X-ray counts vs. energy (keV).

Spectrum 2 shows a **Ni-rich matrix (53 wt%)** with high Cr (18.7 wt%) and Mo (7.35 wt%), indicating a typical Inconel-type chemistry. The **carbon content is very high (15.3 wt%)**, and a small amount of titanium is present. This combination suggests that the region contains **TiC-derived phases**, either as dissolved TiC particles or fine TiC fragments dispersed during deposition. The presence of Nb (4.83 wt%) also confirms the likelihood of NbC carbides. Overall, this area represents a **carbide-rich zone** influenced strongly by TiC reinforcement and WAAM thermal cycles.

Quantitative results

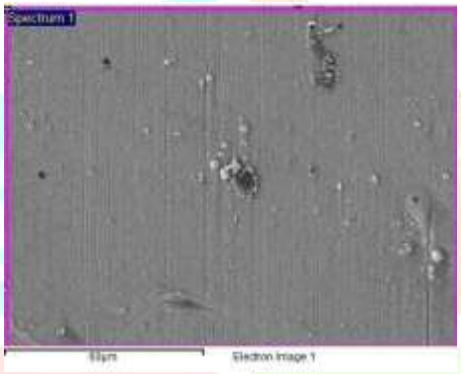

Fig: Electron Image of 3% Tic

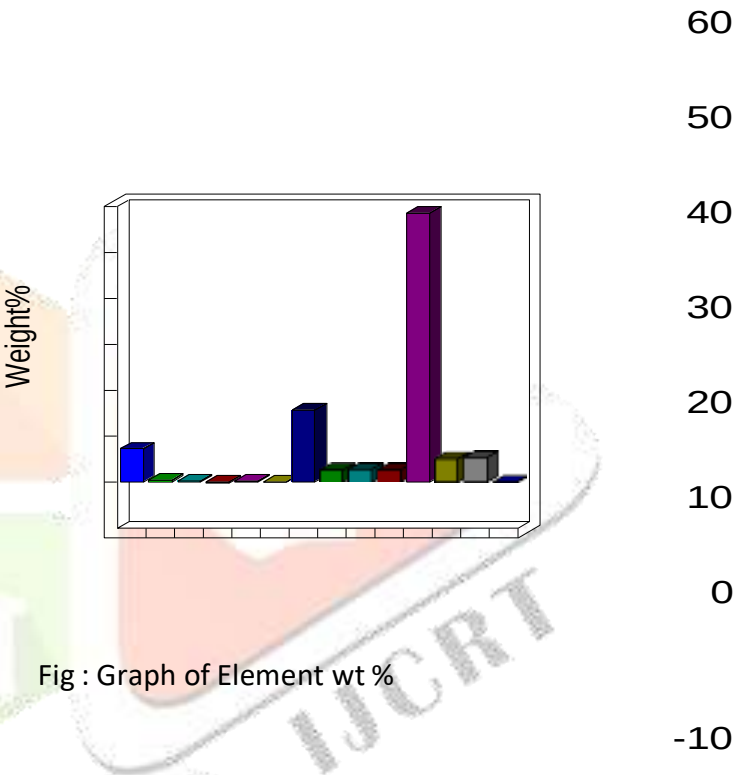

Fig : Graph of Element wt %

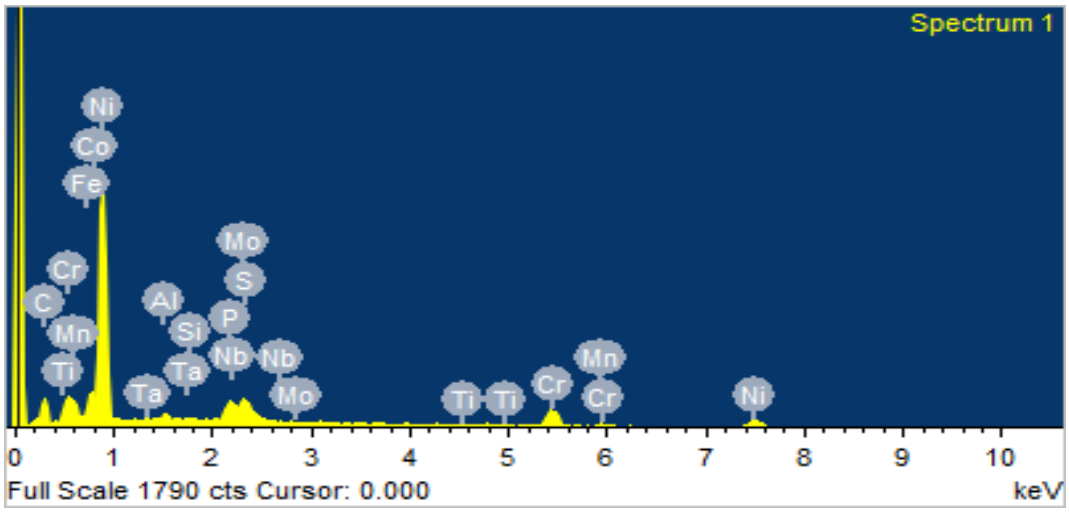

Fig : graph of X-ray counts vs. energy (keV).

Spectrum 1 shows a **Ni-rich matrix (53 wt%)** with high Cr (18.7 wt%) and Mo (7.35 wt%), indicating a typical Inconel-type chemistry. The **carbon content is very high (15.3 wt%)**, and a small amount of titanium is present. This combination suggests that the region contains **TiC-derived phases**, either as dissolved TiC particles or fine TiC fragments dispersed during deposition. The presence of Nb (4.83 wt%) also confirms the likelihood of NbC carbides. Overall, this area represents a **carbide-rich zone** influenced strongly by TiC reinforcement and WAAM thermal cycles.

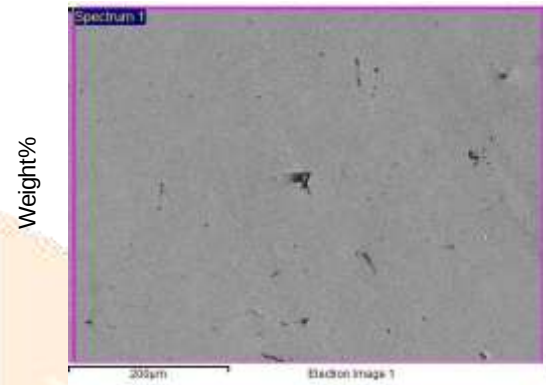

Fig : Electron Image of 4% Tic

Fig : Graph of Element wt %

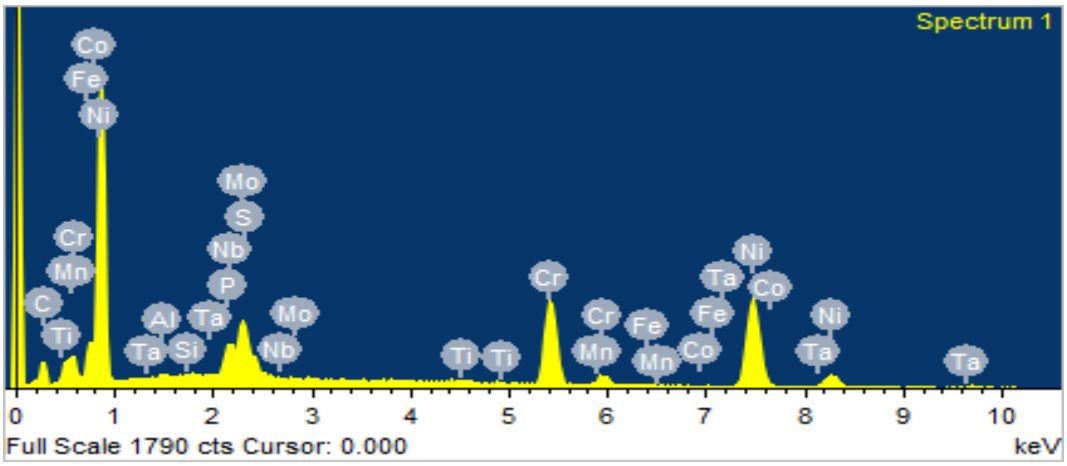

Fig graph of X-ray counts vs. energy (keV).

Spectrum 1 contains **56.4 wt% Ni**, high Cr (19.75 wt%), and the highest Mo content (8.73 wt%) among the three regions. Moderate carbon (9.78 wt%) and measurable titanium (0.34 wt%) confirm the presence of **TiC-influenced microstructure**, though TiC appears more finely dispersed here. Very low Fe, Mn, and Co levels indicate that this area is close to the **pure deposition region**, with minimal dilution. The consistent Nb content (4.97 wt%) suggests stable precipitation hardening through NbC and TiC- related carbides. Overall, Spectrum 3 represents a **uniform alloy region with well- dispersed TiC effects**.

Optical Microscopy:

The optical microscopy images show a clear difference in TiC distribution between the top layer and the inner layers of the WAAM-deposited Inconel 625 composite. In the first image, TiC particles appear evenly distributed across the top surface, indicating that the reinforcement was effectively delivered during the final deposition passes and had limited time to settle or segregate before solidification. However, in the second image representing the inner layers, TiC particles are less uniformly distributed and appear in localized clusters or reduced quantities. This occurs because TiC, having a much higher density and melting point than the molten Inconel, tends to settle, float, or segregate within the melt pool during earlier deposition layers, especially under repeated thermal cycling. Additionally, the reheating from subsequent layers can cause partial dissolution or redistribution of TiC within the inner regions. As a result, the outermost layer retains a more uniform reinforcement distribution, while the inner layers show decreased homogeneity due to melt pool dynamics, particle settling, and thermal remelting effects inherent to the WAAM process.

Fig : 250x magnification

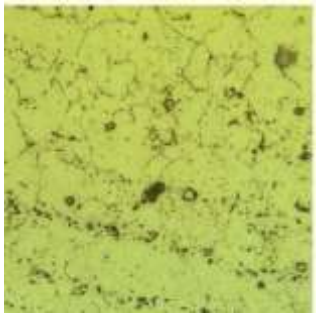

Fig 4: 500x Magnification

MECHANICAL TESTING:

Vickers Hardness:

The hardness of the WAAM-deposited Inconel/TiC composites showed a significant improvement with increasing TiC reinforcement. The ceramic TiC particles acted as strong load-bearing phases and restricted plastic deformation in the metallic matrix, resulting in a progressive rise in hardness from 1% to 4% TiC. The 1% TiC sample exhibited only a slight increase in hardness compared to the control, indicating partial reinforcement due to the limited number of particles distributed within the matrix. With 2% TiC, hardness increased more noticeably as the particle population improved the resistance to indentation. The 3% TiC specimen displayed a sharper improvement, attributed to better particle–matrix bonding and more effective blocking of dislocation motion. The 4% TiC sample showed the highest hardness among all compositions.

Table : Hardness Values

Specimen Name	Results	Percentage
Inc625	280.56	0
Inc625 + 1% TiC	314.06	11.9404049
Inc625 + 2% TiC	332.93	18.66623895
Inc625+ 3% TiC	335	19.40404904
Inc625+ 4% TiC	342.76	22.16994582

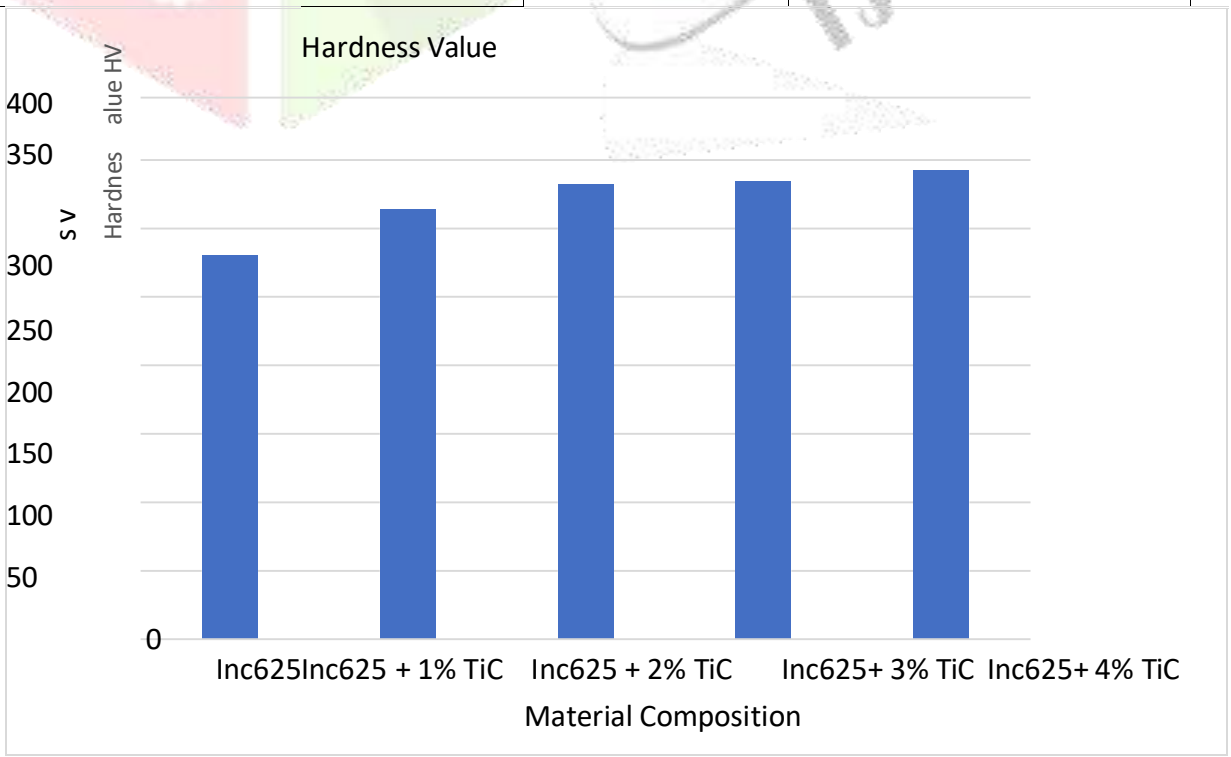

Fig : Hardness Value Graph

Wear Test:

Results Under 3 kg Load.

- 1% and 2% TiC show moderate heating rates, increasing steadily from ~9–10 microns at 0 min to ~250 microns by the end.
- 3% TiC exhibits a higher heat generation, rising sharply and reaching ~245 microns near the end of the cycle, indicating greater frictional interaction.
- 4% TiC displays comparatively lower temperature rise than other TiC contents (only ~181 microns at 318 sec), suggesting improved thermal stability.
- 0% TiC shows the highest temperature values, reaching nearly 300 microns, confirming that TiC addition reduces thermal softening during operation.

Table : Wear at 3kg load

Time(S)	1%TiC	2%TiC	3%TiC	4%TiC	0% TiC
0	9	10	10	6	10
30	10	8	16	14	208
60	22	23	41	4	253
90	46	64	64	15	262
120	63	79	84	33	271
150	84	113	96	61	283
180	105	137	125	84	277
210	126	156	142	101	279
240	145	167	154	122	280
270	180	201	174	136	292
300	226	210	191	149	293
318	250	245	201	181	297

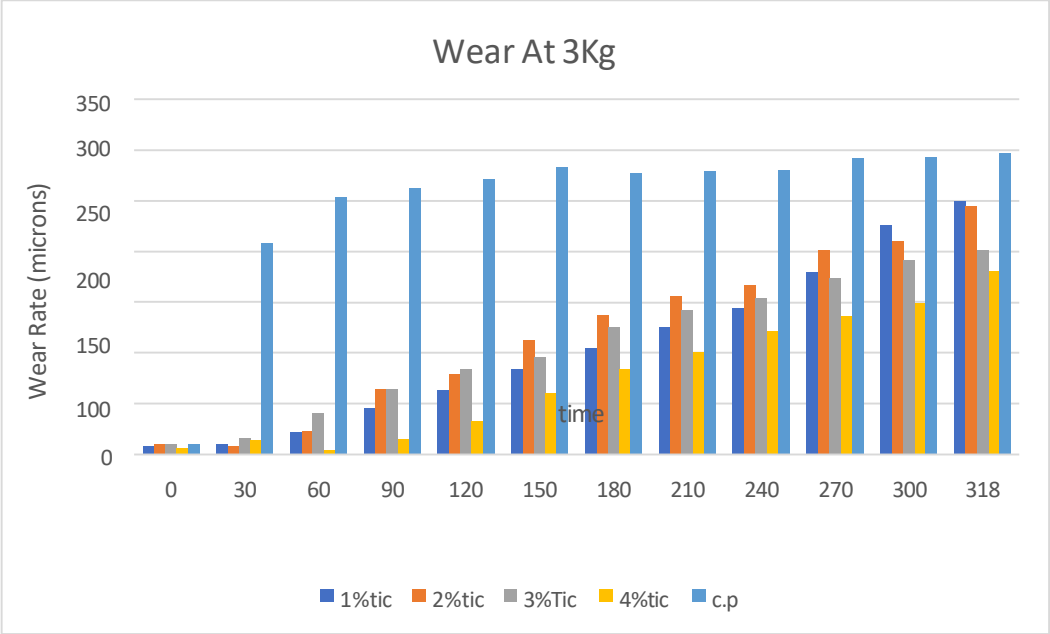

Fig : Graph of Wear at 3kg

Results Under 2 kg Load

- 1% TiC shows a gradual increase in wear from 1 µm to ~61 µm, indicating moderate resistance to material loss.
- 2% TiC displays more stable behaviour with wear rising slowly to a maximum of ~40 µm, showing improved wear resistance compared to lower reinforcement.
- 3% TiC exhibits controlled and moderate wear progression, increasing only to ~34 µm, confirming stable performance under sustained load.
- 4% TiC shows the lowest wear among all compositions, reaching just ~28 µm, demonstrating the highest wear resistance under 2 kg load.
- 0% TiC sample again records the highest wear, rising sharply to ~93 µm, indicating the poorest surface durability without TiC reinforcement.

Table : Wear at 2kg load

Time(S)	1%TiC	2%TiC	3%TiC	4%TiC	0% TiC
0	5	2	10	17	16
30	2	12	25	21	10
60	10	19	5	26	16
90	15	24	8	18	29
120	23	29	10	13	38
150	33	33	24	14	47
180	36	45	24	4	58

210	49	53	39	10	64
240	65	61	51	13	88
270	69	69	66	37	94
300	73	70	69	37	115
318	80	73	71	36	119

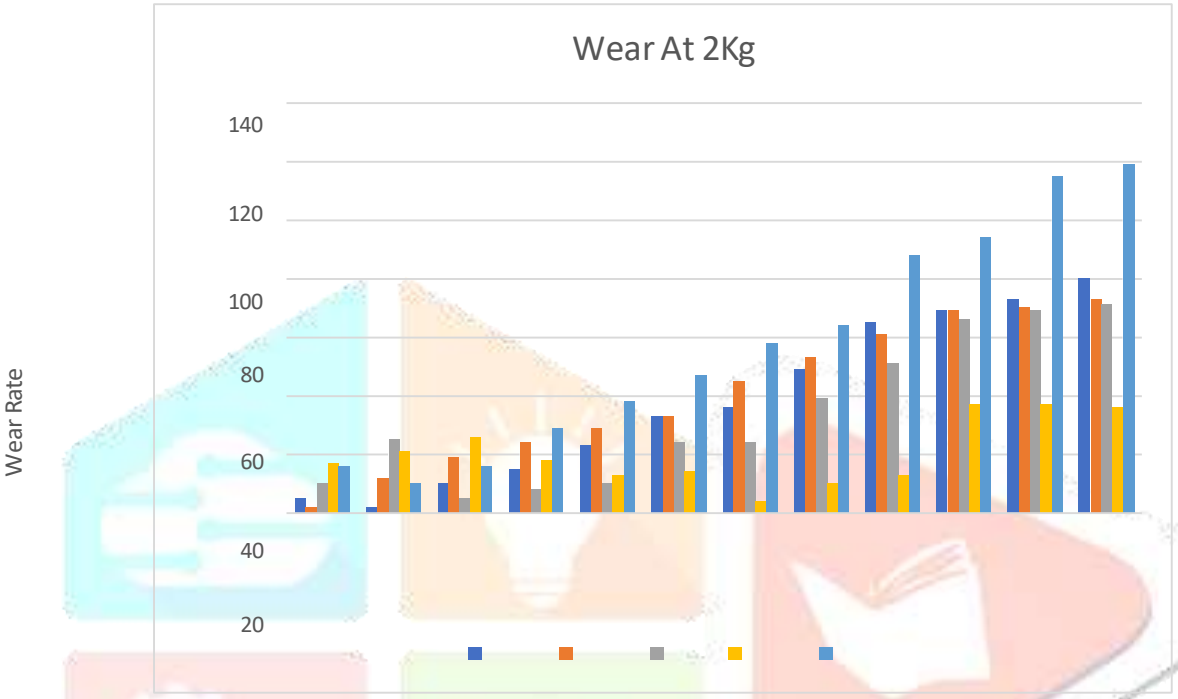

Fig : Wear at 2 kg

Results Under 1 kg Load:

- 1% TiC shows gradual temperature rise from 1 µm to ~61 µm.
- 2% TiC remains relatively stable at lower temperature values (max ~40 µm), indicating good thermal resistance at low loads.
- 3% TiC presents fluctuating but moderate heating (up to ~34 µm), suggesting stable performance.
- 4% TiC remains steady and reaches only ~28 µm, demonstrating the best temperature resistance among all compositions.
- The control sample again records the highest temperatures, reaching ~93 µm, confirming poorer thermal performance.

Table : Wear at 1kg load

Time(S)	1%TiC	2%TiC	3%TiC	4%TiC	0% TiC
0	1	20	30	13	16
30	6	10	24	32	10
60	0	5	20	37	5
90	12	3	15	36	16
120	18	6	10	24	28
150	30	10	5	38	33
180	31	15	9	40	42
210	36	19	11	22	56
240	39	23	20	25	69
270	46	25	25	24	78
300	51	28	30	26	84
318	61	40	34	28	93

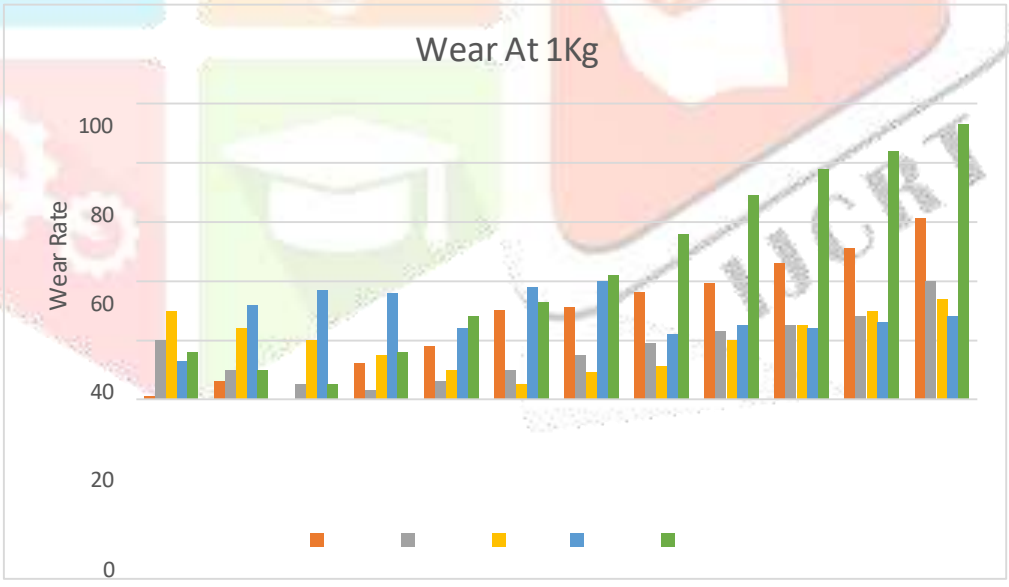

Fig : Wear at 1 kg

Tensile Test:

Tensile test results revealed significant improvements in the mechanical performance of Inconel 625 with the addition of TiC reinforcement. In the vertical build orientation, the unreinforced Inc625 specimen exhibited a tensile strength of 636.3 MPa. The incorporation of TiC particles enhanced the tensile strength across all compositions, with the highest value recorded for the 3% TiC composite at 712.8 MPa. Yield strength also showed a noticeable improvement, reaching a maximum of 431.17 MPa for the 1% TiC

sample. Although elongation values remained relatively high for all compositions, a slight reduction was observed as the TiC content increased, particularly at 4% TiC, indicating a marginal decrease in ductility due to the ceramic phase. In the horizontal orientation, the base Inc625 metal displayed a tensile strength of 656.9 MPa. Similar to the vertical results, TiC reinforcement increased the tensile strength, with the highest value of 708.3 MPa observed for the 2% TiC composite. The yield strength peaked at 475.87 MPa for the 1% TiC sample, suggesting that low levels of TiC contribute effectively to strengthening mechanisms. Elongation percentages remained above 50% in most compositions, except for the 3% TiC specimen, which showed a noticeable drop in ductility. Overall, both tensile strength and yield strength improved with TiC addition, with 1–2% TiC offering the best balance between strength and ductility.

Table : Tensile Test results of Vertical specimen

Tensile Test result				
Specimen Name	**Side**	**Results**		
		Tensile Strength (MPa)	**Yeild Stress (Mpa)**	**Elongation Percentage (%)**
Inc625	Vertical	636.3	376.5	53.44
Inc625 + 1% TiC	Vertical	703.5	431.17	52.69
Inc625 + 2% TiC	Vertical	695.1	426.49	54.5
Inc625+ 3% TiC	Vertical	712.8	415.68	51.44
Inc625+ 4% TiC	Vertical	698.5	384.85	44.38

Table : Tensile test results of Horizontal Specimen

Tensile Test result				
Specimen Name	**Side**	**Results**		
		Tensile Strength (MPa)	**Yeild Stress (Mpa)**	**Elongation Percentage (%)**
Inc625	Horizontal	656.9	414.23	54.69
Inc625 + 1% TiC	Horizontal	686.9	475.87	52.75
Inc625 + 2% TiC	Horizontal	708.3	387.37	54.13
Inc625+ 3% TiC	Horizontal	633.8	388.88	42.63

Inc625+ 4% TiC	Horizontal	638	394.01	57.63

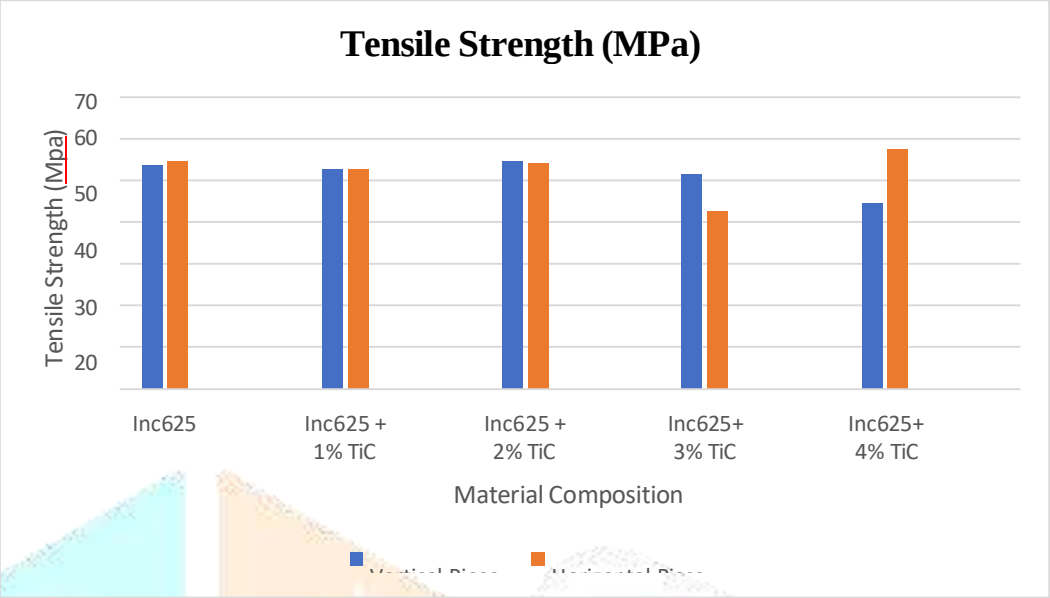

Fig 4.18: Graph comparison of vertical and horizontal tensile values

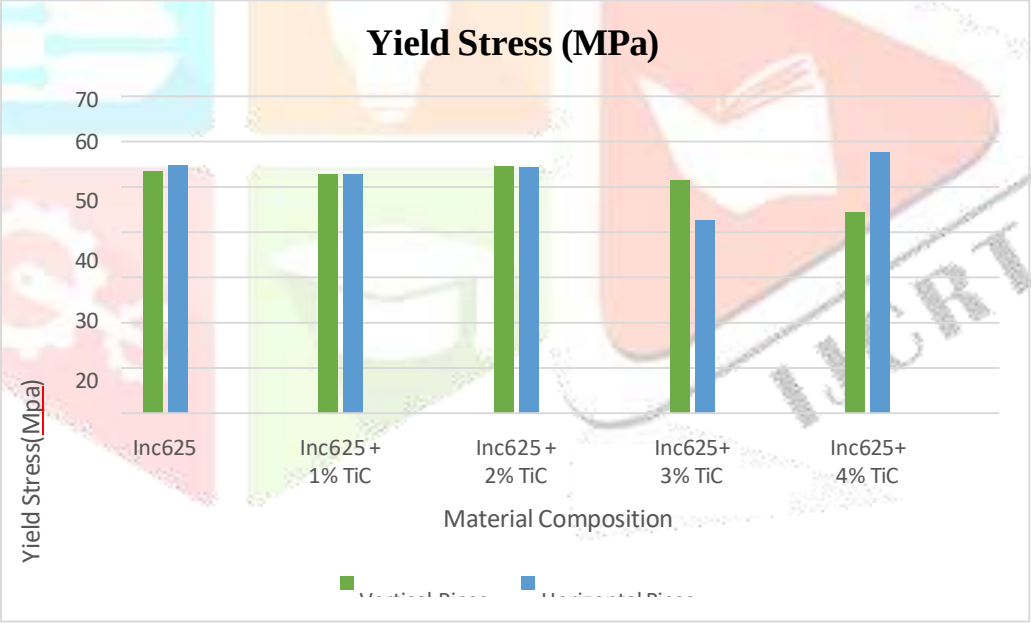

Fig : Graph comparison of vertical and horizontal Yield Stress values

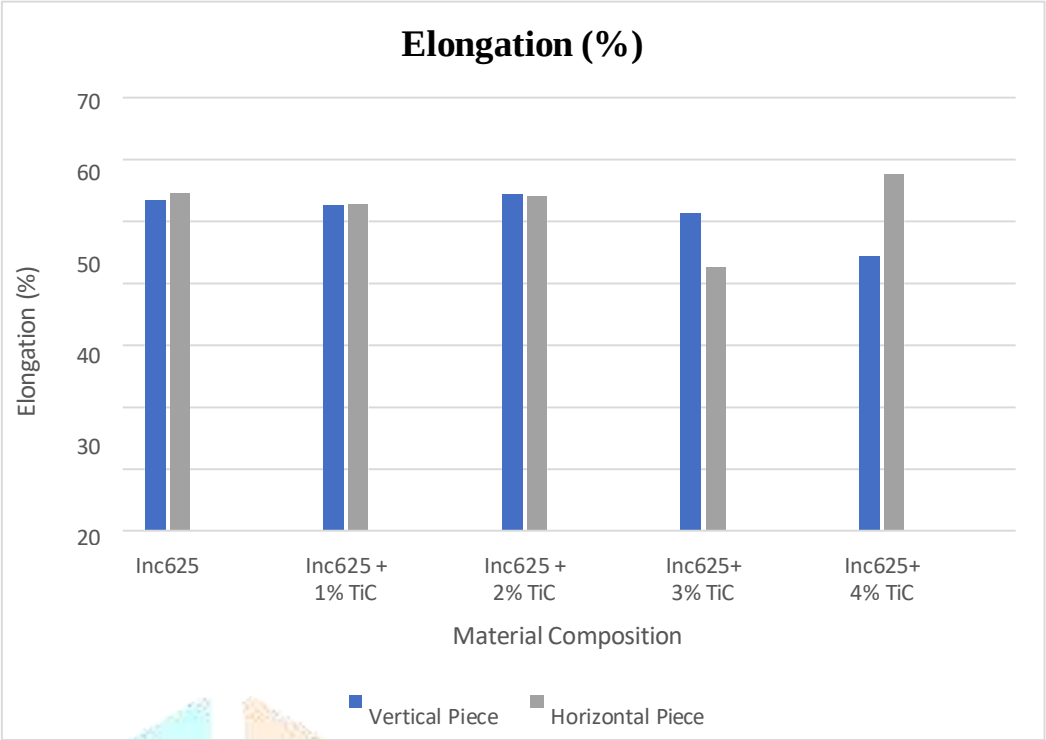

Fig 4.20: Graph comparison of vertical and horizontal Elongation values

Impact Test:

The impact test results revealed a clear contrast in behaviour between the unreinforced and TiC-reinforced Inconel 625 samples. The unreinforced Inconel 625 exhibited the highest impact energy of 121.1 J, demonstrating its inherent toughness and excellent ability to absorb energy under high-strain-rate loading. This aligns with the known ductile nature of Inconel 625, which maintains good fracture resistance due to its solid- solution strengthening and stable austenitic microstructure. With the introduction of TiC particles, a noticeable reduction in impact toughness was observed across all reinforced samples. This decline can be attributed to the brittle nature of ceramic reinforcements, which tend to act as stress concentrators during impact loading. Among the reinforcements, the 2% TiC composite showed the lowest impact energy value of

52.3 J, indicating that poor particle distribution or localized clustering may have contributed to premature crack initiation. Interestingly, the 4% TiC sample displayed a partial recovery in impact strength, reaching 73.6 J. This improvement may be associated with enhanced particle dispersion or refinement in the microstructure, which helped mitigate crack propagation to some extent.

Table : Impact Test Values

Impact Test	
Specimen Name	**Results**
Inc625	121.1
Inc625 + 1% TiC	103.5
Inc625 + 2% TiC	52.3
Inc625+ 3% TiC	53.4
Inc625+ 4% TiC	73.6

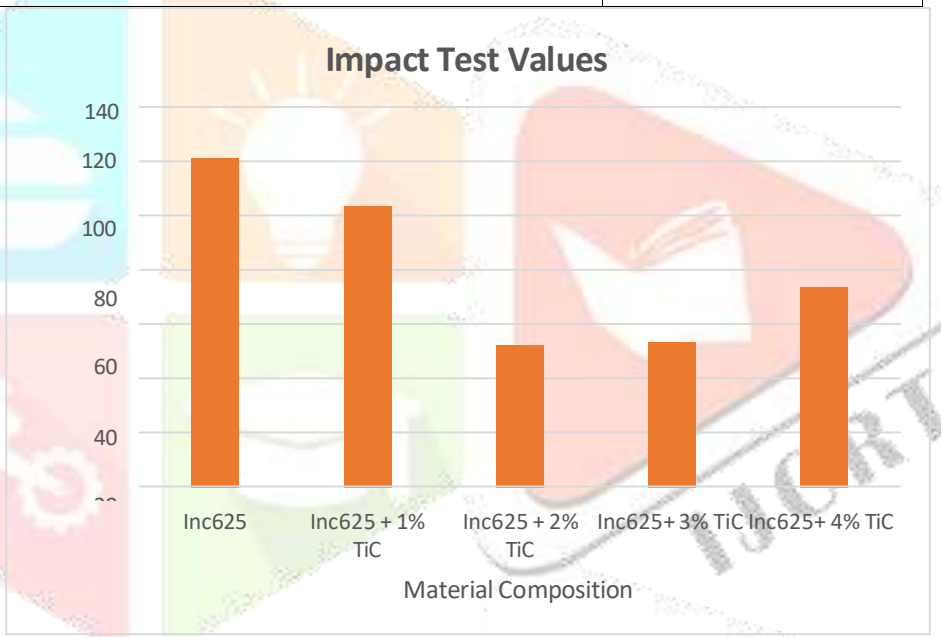

Fig 4.21: Graph comparison of Impact Test values

CONCLUSION

Inconel 625 composites reinforced with 1–4 wt.% TiC were successfully fabricated using the Wire Arc Additive Manufacturing (WAAM) process. The deposition remained stable throughout, and the in-situ addition of TiC powder through a feeder enabled uniform dispersion within the molten pool, producing sound and defect-free walls with strong metallurgical bonding between layers. Microstructural examination confirmed that TiC particles refined the grain morphology, restricted grain boundary movement, and contributed to strengthening through dispersion hardening and grain boundary pinning. However, at reinforcement levels above 3 wt.%, localized particle agglomeration and micro void formation were observed, slightly reducing ductility and toughness.

Mechanical testing showed that TiC reinforcement significantly improved hardness and tensile behaviour. Vickers hardness increased steadily from 280.56 HV for the base alloy to 342.76 HV at 4 wt.% TiC, representing an approximate 22% enhancement. This improvement was attributed to the load-transfer effect from hard TiC particles and the refined microstructure. The ultimate tensile strength (UTS) increased notably with TiC addition, reaching a maximum of 712.8 MPa at 3 wt.% TiC compared to 636.3 MPa for unreinforced Inconel 625. Yield strength followed the same trend, while elongation decreased slightly, indicating that the incorporation of ceramic particles reduced ductility but did not severely compromise deformation capability. These findings demonstrate that 2–3 wt.% TiC provides an optimal balance between strength enhancement and acceptable ductility before brittleness becomes dominant.

In contrast, impact toughness showed a declining trend with reinforcement. The base alloy exhibited the highest impact energy of 121.1 J, confirming its excellent toughness. The addition of TiC reduced absorbed energy to approximately 52–73 J due to the brittle nature of ceramic particles and decreased plastic deformation capacity. The lowest value, 52.3 J, occurred at 2 wt.% TiC, while a slight improvement at 4 wt.% TiC (73.6 J) suggested better particle distribution or microstructural adjustments at higher reinforcement levels.

Wear performance improved significantly across all reinforced samples. The 4 wt.% TiC composite exhibited the lowest cumulative wear loss, showing up to a 32% reduction compared to the base alloy under identical testing conditions. This enhancement resulted from the high hardness and stability of TiC particles, which act as load-bearing reinforcements and reduce material removal during sliding. The improved wear resistance further confirms the beneficial role of TiC in strengthening the composite matrix.

Overall, the study concludes that TiC reinforcement during WAAM processing offers a viable and cost-effective method to produce high-strength, wear-resistant nickel-based components. Among all compositions tested, 3 wt.% TiC was identified as the most effective reinforcement level, providing excellent hardness, tensile strength, and wear resistance while maintaining acceptable ductility and process stability. These findings highlight the potential of WAAM-based TiC-reinforced Inconel 625 composites for advanced aerospace, marine, chemical, and high-temperature applications.

REFERENCES

[1] Rooprai, R.S., Bansal, A., Singh, J. “Influence of TiC powder content on wear behaviour of Inconel 625 clads developed by hybrid-mode wire arc additive manufacturing (WAAM) on EN-8 steel.” Tribology International, 189 (2023) 108937.

[2] Rodrigues, T.A., Malfeito, A., Farias, F.W.C., Duarte, V., Lopes, J., Filho, J.C.P., Avila, J.A., Schell, N., Santos, T.G., Oliveira, J.P. “Grain refinement of Inconel 625 during wire-based directed energy deposition additive manufacturing by in-situ added TiB_2 particles.” Intermetallics, 175 (2024) 108540.

[3] Bölükbaşı, Ö.S., Serindağ, T., Gürol, U., Günen, A., Çam, G. “Improving oxidation resistance of wire arc additive manufactured Inconel 625 Ni-based superalloy by pack aluminizing.” CIRP Journal of Manufacturing Science and Technology, 46 (2023) 89– 97.

[4] Sharma, H., Singla, J., Singh, V., Singh, J., Kumar, H., Bansal, A., Singla, A.K., Goyal, D.K., Gupta, M.K. “Influence of post heat treatment on metallurgical, mechanical, and corrosion analysis of wire arc additive manufactured Inconel 625.” Journal of Materials Research and Technology, 27 (2023) 5910–5923.

[5] Rodrigues, T.A., Farias, F.W.C., Zhang, K., Shamsolhodaei, A., Shen, J., Zhou, N., Schell, N., Capek, J., Polatidis, E., Santos, T.G., Oliveira, J.P. "Wire and arc additive manufacturing of 316L stainless steel/Inconel 625 functionally graded material: Development and characterization." Journal of Materials Research and Technology, 21 (2022) 237–251.

[6] Amiri, V., Naffakh-Moosavy, H. "Wire arc additive manufacturing of functionally graded carbon steel–stainless steel 316L–Inconel 625: Microstructural characterization and mechanical behavior." Journal of Advanced Joining Processes, 9 (2024) 100194.

[7] Kishor, G., Mugada, K.K., Mahto, R.P., Sivanandam, A., Digavalli, R.K., Amirthalingam, M. "Microstructural evolution, crystallographic texture, grain morphology, and mechanical integrity of wire arc additively manufactured Inconel 625 alloy." Materials Characterization, 218 (2024) 114525.

[8] Gurmesa, F.D., Lemu, H.G., Tucho, W.M., Akessa, A.D. "Effects of wire diameter on mechanical and microstructural properties of Inconel 625 fabricated by wire arc additive manufacturing." Journal of Materials Research and Technology, 35 (2025) 3226–3235.

[9] Chen, X., Han, J., Wang, J., Cai, Y., Zhang, G., Lu, L., Xin, Y., Tian, Y. "A functionally graded material from TC4 to 316L stainless steel fabricated by double- wire + arc additive manufacturing." Materials Letters, 300 (2021) 130141.

[10] Zhang, W., Wang, J., Zhu, X., Lu, X., Ling, X. "A functionally graded material from stainless steel 304 to Fe–40Al fabricated by dual wire arc additive manufacturing." Journal of Materials Research and Technology, 28 (2024) 3566–3572.

[11] Günen, A., Gürol, U., Koçak, M., Çam, G. "A new approach to improve some properties of wire arc additively manufactured stainless steel components: Simultaneous homogenization and boriding." Surface & Coatings Technology, 460 (2023) 129395.

[12] Shah, A., Aliyev, R., Zeidler, H., Krinke, S. "A review of the recent developments and challenges in wire arc additive manufacturing (WAAM) process." Journal of Manufacturing and Materials Processing, 7 (2023) 97.

[13] Kong, Y., Peng, K., Huang, H. "Additive manufacturing of high-strength Inconel 718 alloy through the addition of Ti_2AlC MAX particles." Journal of Materials Science & Technology, 158 (2023) 180–193.

[14] Cai, X., Wang, Z., Dong, L., Yang, M., Zhou, J., Xue, F. "Advanced mechanical properties of nickel–aluminum bronze/steel composite structure prepared by wire-arc additive manufacturing." Materials & Design, 221 (2022) 110969.

Rashid, M., Sabu, S., Kunjachan, A., Agilan, M., Anjilivelil, T., Joseph, J. "Advances in wire-arc additive manufacturing of nickel-based superalloys: Heat sources, DfAM principles, material evaluation, process parameters, defect management, corrosion evaluation and post-processing techniques." International Journal of Lightweight Materials and Manufacture, 7 (2024) 882–913.